EDGE2D-EIRENE and ERO2.0 predictions of nitrogen molecular break-up and transport in the divertor of JET low-confinement mode plasmas

R. Mäenpää[a,*], H. Kumpulainen[a], M. Groth[a], J. Romazanov[b], B. Lomanowski[c], S. Brezinsek[b], S. Di Genova[e], J. Karhunen[d], K. Lawson[d], A. G. Meigs[d], S. Menmuir[d], A. Shaw[d] and JET Contributors[**]

[a]*Aalto University, Espoo, Finland*
[b]*Forschungszentrum Jülich GmbH, Jülich, Germany*
[c]*Oak Ridge National Laboratory, Oak Ridge, TN, USA*
[d]*UKAEA, Culham Science Centre, Abingdon, United Kingdom*
[e]*Aix-Marseille Univ, Marseille, France*

roni.maenpaa@aalto.fi

Abstract

EDGE2D-EIRENE simulations of nitrogen-seeded partially detached JET L-mode plasmas show that the divertor N I to N V radiation distributions are highly sensitive to the upstream electron density, and less sensitive to changes in the assumed cross-field particle diffusivity for nitrogen ions. The EDGE2D-EIRENE simulations reproduce the peak intensities of N I to N V as measured by vertically viewing divertor spectrometers to within 50% for a narrow range of the upstream electron density within the experimental uncertainties, while the predicted profiles are narrower than the measured ones. Including nitrogen atoms only in the ERO2.0 simulations implies an up to a factor of five lower N III and N IV intensities compared to EDGE2D-EIRENE. If nitrogen is assumed to recycle exclusively as molecules instead of atoms, ERO2.0 predicts that the N II, N III and N IV intensities in the divertor increase by up to a factor of four and that the time-averaged, volume-integrated number of N^{7+} ions in the plasma increases by approximately a factor of 5.

Word count: 168

Keywords: nitrogen emission, JET, EDGE2D-EIRENE, ERO2.0

**Corresponding author address:* Aalto University, Otakaari 1, 02150 Espoo, Finland

*Corresponding author e-mail: roni.maenpaa@aalto.fi

Presenting author: Roni Mäenpää

Presenting author e-mail: roni.maenpaa@aalto.fi

**See the author list of 'Overview of JET results for optimising ITER operation' by J. Mailloux et al. to be published in Nuclear Fusion Special issue: Overview and Summary Papers from the 28th Fusion Energy Conference (Nice, France, 10-15 May 2021)

I. Introduction

Nitrogen impurity injection has been used in the ASDEX Upgrade and JET tokamaks to achieve simultaneous high confinement, high radiated power fraction and detached divertor operation with suppressed edge localized modes (ELMs) [1, 2]. However, deuterated ammonia production has been observed during nitrogen seeded discharges in both ASDEX Upgrade and JET [3, 4]. In future tokamaks such as ITER, tritiated ammonia formation during plasma operation may necessitate high-temperature regeneration of the cryopump system with a significant impact on the duty cycle of the device [5]. Recently, stable plasmas with high confinement and suppressed ELMs have also been demonstrated at JET using neon injection, but these plasmas have not achieved detached divertor conditions [6].

To better understand nitrogen transport in the divertor, the sensitivity of EDGE2D-EIRENE [7, 8] simulations of nitrogen-seeded, partially-detached, low-confinement mode (L-mode) plasmas in JET, previously presented in [9], to the upstream electron density and the cross-field particle diffusivity of nitrogen ions is studied. The EDGE2D-EIRENE simulation with the best agreement between the predicted and measured N I - N V intensities in the divertor is used in ERO2.0 [10] simulations as a background plasma to study the impact of nitrogen molecular dissociation reactions.

Previously, it was reported that ERO2.0 predicts an increase in the divertor N II and N III line emission when nitrogen is assumed to recycle as molecules instead of atoms, as well as an increase of up to 50% in the N^{2+} ion content in the plasma [11]. The new ERO2.0 simulations include corrections to the temperature gradient force calculation in ERO2.0, which allow us to extend the analysis to medium and high charge-states (3+ to 7+), which were previously excluded due to numerical artefacts proportional to Z^2 arising during the temperature gradient force calculation.

II. Nitrogen intensity measurements in partially detached JET L-mode plasmas

Nitrogen-seeded ELM-free JET L-mode discharges, JET pulse numbers (JPN) 90416-90423, with a divertor strike point geometry optimized for diagnosis of the low-field side (LFS) divertor (see Fig. 1 in [9]), including measurements of multiple nitrogen lines in different charge states, were chosen as the source of experimental data. From the nitrogen-seeding scan, JPN 90422 and 90423 employed the highest N seeding rate ($1.6 \cdot 10^{21}$ N atoms per second) which did not result in a plasma disruption. The toroidal magnetic field was 2.5 T, the plasma current 2.5 MA, and the ion $\mathbf{B} \times \nabla$B-drift pointed into the divertor. The plasmas were heated with 1.6 MW of Ohmic power and 1.8 MW of neutral beam injection power. Nitrogen was injected using a toroidally distributed gas injection module located in the LFS scrape-off layer and approximately 10 cm radially outboard from the LFS strike point (see Fig. 1 in [9]).

The spectroscopic setup of JET discharges 90416-90423 for nitrogen was extensively characterized in [12]. A low-resolution, visible spectrometer with a single vertical line-of-sight centered on the LFS horizontal target plate (JET system KS8) was used to measure near-infrared N I and visible N II emission [13]. Near-ultraviolet radiation from N II, N III and N IV was measured using the high-resolution, mirror-link divertor spectroscopy system (KT3), which includes 22 vertical lines-of-sight into the divertor coupled to three high-resolution spectrometers [14]. Extreme ultraviolet radiation from N V was measured by the poloidally scanning spectrometer system (KT1) [15]. Mirror-based divertor-viewing endoscope cameras (KL11) were used in conjunction with tomographic reconstructions to measure the 2D poloidal distribution of N II emission at 500.6 nm [16, 17]. N II emission at 500.6 nm was also measured using the vertically viewing fibre optic divertor filterscope (KS3O) [18].

III. Setup of EDGE2D-EIRENE and ERO2.0 simulations

The EDGE2D-EIRENE simulations of deuterium-beryllium-nitrogen plasmas (ca. 0.5% Be and 0.15%-0.4% N content) used in this work are based on the simulations described in [9].

The simulations in [9] were configured with the aim to match the plasma conditions upstream and in the LFS divertor in the experimental unseeded deuterium-only reference pulse. The approach in this work was to adjust the electron density at the separatrix at the LFS midplane ($n_{e,\,sep,\,LFS\text{-}mp}$) and the cross-field particle diffusivity for nitrogen ions to reproduce the nitrogen spectroscopic measurements in the LFS divertor in the pulses with the highest nitrogen seeding rate with EDGE2D-EIRENE predictions. Apart from these changes the EDGE2D-EIRENE simulation setup is identical to that in [9].

From lithium-beam and high-resolution Thomson scattering measurements $n_{e,\,sep,\,LFS\text{-}mp}$ was previously estimated to be between $2.0{\cdot}10^{19}$ m^{-3} and $2.2{\cdot}10^{19}$ m^{-3} [19]. In this work, $n_{e,\,sep,\,LFS\text{-}mp}$ is reduced to $1.9{\cdot}10^{19}$ m^{-3} (to obtain better agreement between code prediction and experiment) and held constant in the simulations using feedback D_2 injection from the private-flux region. The cross-field particle diffusivity $D_\perp$ for deuterium is set to 1.0 $m^2\,s^{-1}$ in the entire computational domain, except in the private-flux region and in a 2 cm-wide region around the separatrix where it is reduced to 0.5 $m^2\,s^{-1}$. In [9], the particle diffusivities of nitrogen ($D_{\perp,\,N}$) and beryllium ($D_{\perp,\,Be}$) were set equal to that of deuterium. In this work, $D_{\perp,\,N}$ is assumed spatially constant and systematically varied from $D_{\perp,\,N}$ = 1.0 $m^2\,s^{-1}$ to 10.0 $m^2\,s^{-1}$. $D_{\perp,\,Be}$ is kept equal to that of deuterium. The thermal diffusivity for ions (χ_i) is set to 1.0 $m^2\,s^{-1}$ inside the separatrix and is reduced to 0.5 $m^2\,s^{-1}$ in the scrape-off layer and in the private-flux region, whereas the thermal diffusivity for electrons (χ_e) is reduced to 0.5 $m^2\,s^{-1}$ in the scrape-off layer only. The particle pinch velocity is set to zero for deuterium, nitrogen and beryllium as in [9]. The input power from the core to the edge plasma is set to 3.2 MW, assuming that 200 kW only are radiated inside the core plasma. Nitrogen is assumed to be a fully recycling species which recycles as atoms. Beryllium is included in the simulations as a non-recycling impurity, and its source at the main chamber is determined by physical erosion as predicted by EIRENE. The divertor plates are assumed to be tungsten. However, tungsten sputtering and transport is omitted in these simulations. The cross-field drift terms are not activated in these simulations due to particle and momentum conservation issues. Due to the large influence of

drifts on the plasma solution in the high-field side (HFS) divertor and the superior spectroscopic coverage of the LFS divertor, the analyses focus on the LFS divertor only. All EDGE2D-EIRENE runs are post-processed using the pyproc-code [9].

To investigate the effect of nitrogen molecular dissociation reactions on nitrogen transport, the 3D kinetic Monte Carlo trace impurity code ERO2.0, which includes a set of five nitrogen molecular ionization and dissociation reactions like its predecessor ERO1.0 [20], is employed. Currently, it is not possible to simulate nitrogen molecules in EDGE2D-EIRENE. The nitrogen molecular reaction rate data in ERO2.0 are based on experimental measurements of reaction cross-sections [21, 22, 23]. In ERO2.0, the dissociation fragments of molecules and molecular ions gain a total of 2.0 eV of translational energy. The constant value 2.0 eV is an approximation, as in experiments a distribution of energies is measured depending on the specific reaction. Translational energy releases as high as 11.8 eV have been measured in the dissociative ionization of N_2^+ [23].

To simulate nitrogen transport using ERO2.0, the background plasma data (n_e, T_e, T_i, v_{par}, $\mathbf{B}$, E_{par}, $q_{par,\,cond}$) from EDGE2D-EIRENE are used. To convert the background plasma data from the magnetically aligned grid of EDGE2D-EIRENE to a Cartesian grid in the poloidal plane, bilinear interpolation is used. EDGE2D-EIRENE assumes toroidal symmetry, and therefore there is no toroidal variation in the background plasma data for ERO2.0. Exponential extrapolation is used to extend the background plasma data to the device wall, as the EDGE2D-EIRENE computational domain does not extend radially to the device wall in the scrape-off layer. ERO2.0 internally accounts for $\mathbf{E} \times \mathbf{B}$ and $\mathbf{B} \times \nabla B$ drifts by virtue of the Boris-method. The radial electric field was not included in the ERO2.0 simulations to keep the EDGE2D-EIRENE and ERO2.0 simulations as comparable as possible. The ERO2.0 version used in this work also includes a kinetic calculation of the parallel temperature gradient force based on equation (12) in [24]. Only the parallel part is included in our simulations. Previously, including the parallel temperature gradient force in ERO2.0 produced

numerical artefacts (unphysical cross-field motion of ions) due to errors in calculating the parallel temperature gradient which have now been resolved.

Three different ERO2.0 cases were run, all using the same deuterium-beryllium-nitrogen plasma from EDGE2D-EIRENE. In the first case ("atoms only"), nitrogen is injected as neutral atoms and all nitrogen ions recycle as atoms. In the second case ("molecular injection"), nitrogen is injected as N_2, but molecules dissociate upon impact with a wall and nitrogen ions recycle as atoms. In the third case ("molecular injection and recycling"), N_2 is injected, atoms recombine into N_2 upon wall impact and N ions recycle as N_2. In all three cases, the same amount of nitrogen was injected (measured by the number of atoms, each N_2 molecule counting as two atoms). In all ERO2.0 runs, the injected molecules and atoms, as well as the atoms and molecules recycling from walls have a constant kinetic energy of 0.025 eV.

IV. Comparison of the measured and EDGE2D-EIRENE predicted line intensities

At an upstream electron density of $2.0 \cdot 10^{19}$ m^{-3}, EDGE2D-EIRENE predicts that the N II 500.6 nm emission peak is located next to the X-point in the low-field scrape-off layer, with the emission localized almost entirely within two computational grid cells (Fig. 1). This observation is qualitatively inconsistent with tomographic reconstructions of the KL11 camera data, which show the peak N II 500.6 nm emission in the low-field side divertor leg approximately half-way between the target and the X-point. Reducing the upstream electron density to $1.9 \cdot 10^{19}$ m^{-3}, still within the uncertainty of the measured $n_{e,\ sep,\ LFS\text{-}mp}$, allows EDGE2D-EIRENE to reproduce the location of the N II peak emission consistent with the tomographic reconstructions. The accuracy of the tomographic reconstruction is confirmed by comparing the radial intensity profiles obtained by integrating through the reconstruction with the intensity profile measured by the vertically viewing fibre optic divertor spectrometer (Fig. 2).

Reducing the upstream electron density from $2.0 \cdot 10^{19}$ m^{-3} to $1.9 \cdot 10^{19}$ m^{-3} also moves the predicted radial locations of N II (404.2 nm), N III (410.1 nm) and N IV (348.2 nm) peak intensities, as determined by the vertical divertor spectrometer, radially outward by approximately 10 cm. At an upstream electron density of $1.9 \cdot 10^{19}$ m^{-3}, the peak intensity of N II predicted by EDGE2D-EIRENE is within 50% of the value measured by the vertically viewing KT3 divertor spectrometer (Fig. 3). For N III and N IV, the EDGE2D-EIRENE predictions are within 50% and 15%, respectively, of the measured peak intensities.

EDGE2D-EIRENE consistently overestimates the N I (747.4 and 821.4 nm) and underestimates N II (500.6 and 648.3 nm) intensities when the synthetic diagnostic predictions are compared to experimental measurements with the KS8D vertically viewing spectrometer system (Fig. 4). The best agreement between measurement and EDGE2D-EIRENE prediction is obtained when $n_{e,\,sep,\,LFS\text{-}mp}$ is set to $1.9 \cdot 10^{19}$ m^{-3}. The simulations show that the N I intensity is determined by electron-impact excitation; free-electron recombination contributes approximately 10% to the N I intensity. For the higher charge states, the predicted contribution from free-electron recombination is negligible. EDGE2D-EIRENE predictions of extreme ultraviolet N V (26.6 nm) intensity agree to within 10% with measurements by the KT1 vertically viewing, poloidally scanning spectrometer (Fig. 5). EDGE2D-EIRENE predicts that the N V emission peak is located ca. 2-3 cm radially outward from the experimentally measured peak emission.

Setting $D_{\perp,\,N}$ to a spatially constant value of 1.0 $m^2\,s^{-1}$ (including in the area around the separatrix and in the private flux region) improves the agreement between the experimentally measured N II, N III and N IV intensities and the EDGE2D-EIRENE prediction when the upstream electron density is set to $1.9 \cdot 10^{19}$ m^{-3}. For this reason, the parameter scans of $D_{\perp,\,N}$ in this work use spatially constant values. For higher upstream electron densities, the effect of setting $D_{\perp,\,N}$ to a spatially constant value of 1.0 $m^2\,s^{-1}$ is negligible.

For the three charge states N II, N III and N IV, EDGE2D-EIRENE underestimates the intensities radially outward from the emission peak. Increasing the cross-field particle

diffusivity for nitrogen $D_{\perp, N}$ (up to 10.0 $m^2 s^{-1}$) does not significantly broaden the emission distribution, but rather increases the peak emission for N III and N IV. This effect is the most substantial for N III emission, where increasing $D_{\perp, N}$ from 1.0 $m^2 s^{-1}$ to 10.0 $m^2 s^{-1}$ produces a factor of two increase in the peak intensities. N I and N V emission is reduced when $D_{\perp, N}$ is increased. The nitrogen impurity fraction of the plasma is decreased from 0.4% to 1.5% when $D_{\perp, N}$ is increased from 1.0 $m^2 s^{-1}$ to 10.0 $m^2 s^{-1}$ for all upstream densities. The best agreement between the EDGE2D-EIRENE predictions of N II emission at 500.6 nm and the tomographic reconstructions of KL11 camera data is achieved when $D_{\perp, N}$ is set to 5.0 $m^2 s^{-1}$ and $n_{e, sep, LFS-mp}$ is set to $1.9 \cdot 10^{19}$ m^{-3}.

The measured N II, N III and N IV intensities peak approximately 5 cm radially inward of the intensity peak predicted by EDGE2D-EIRENE at $n_{e, sep, LFS-mp} = 1.9 \cdot 10^{19}$ m^{-3} and $D_{\perp, N} = 1.0$ $m^2 s^{-1}$. Increasing $D_{\perp, N}$ moves the N II emission peak radially inward and thus improves the agreement with experiment, but increases N IV intensity, leading to an overprediction of that line. It is therefore difficult to judge which value of $D_{\perp, N}$ provides the best agreement with experiment, as not all charge states can be matched simultaneously. An EDGE2D-EIRENE simulation that provides a balanced match to the experimental data with respect to the different charge states was used to generate the background plasma for the ERO2.0 simulations ($n_{e, sep, LFS-mp} = 1.9 \cdot 10^{19}$ m^{-3} and $D_{\perp, N} = 1.0$ $m^2 s^{-1}$).

V. Impact of nitrogen recycling as atoms versus molecules studied with ERO2.0

If nitrogen atoms only are included in the ERO2.0 simulations, ERO2.0 underestimates the N I intensity by approximately 50%, decreasing to 20% for N II and increasing to 70-80% for N III to N V (Figs. 3-5). It is hypothesized that this discrepancy, which is largest for N III and N IV (charge states 2+ and 3+), is caused by the different treatment of temperature gradient forces in EDGE2D-EIRENE and ERO2.0.

The codes which assume instantaneous thermalization of impurity ions with respect to the main ion temperature, such as EDGE2D-EIRENE, have been shown to overestimate the

magnitude of thermal forces acting on impurity ions in intermediate charge states (2+ to 3+) near the targets [25, 26]. This overestimation leads to enhanced parallel transport of the impurity ions away from the target, and it is hypothesized here that this also results in higher emission by electron-impact excitation. The overestimation is less significant for the singly charged ions, which are very short-lived, and for the ions in higher charge states (≥ 4+) which have had more time to thermalize. The kinetic treatment of the temperature gradient forces in ERO2.0 does not lead to such an overestimation. Disabling the temperature gradient force in ERO2.0 altogether leads to a factor of two lower peak intensities for N II to N V in the atoms only-case.

If nitrogen gas is injected as molecules, but all nitrogen recycles as atoms and all N_2 molecules dissociate upon wall impact, the increase in the N II to N V peak intensities and the decrease for N I is negligible (within one standard deviation of the reference "atoms only" case). The negligible effect of molecular injection results from the fact that the recycling source is approximately two orders of magnitude greater than the injection source. Correspondingly, the concentration of molecules in the "molecular injection" case is approximately two orders of magnitude lower than in the "molecular injection and recycling" case.

If all nitrogen is assumed to recycle as molecules and all atoms recombine into molecules upon wall contact in ERO2.0, the peak N II intensity is increased by approximately a factor of two compared to the atoms only-case. For N III, N IV and N V, the peak intensities are increased by approximately a factor of four, two and two, respectively. ERO2.0 predicts that N I intensity is reduced by approximately 66% (747 nm spectral line) to 80% (822 nm spectral line) under the assumption of molecular recycling. Monte Carlo noise for the two highest charge states studied here (N IV and N V) is high relative to the difference between the three cases, in particular at locations radially inward from the measured emission peaks ($R < 2.6$ m). If the translational energy gain by the dissociation fragments is set to zero for all reactions and nitrogen ions are assumed to recycle as molecules, the N II, N III and N IV

intensities are reduced by approximately 50% compared to the atoms only case, likely due to the lower thermal velocity and poorer plasma penetration of the nitrogen molecules.

Assuming molecular recycling of nitrogen decreases the time-averaged, volume-integrated number of N^+ ions in the plasma by approximately 25% (Fig. 6) due to the combined effect of N_2^+ being created instead of N^+ and the fast dissociation fragments being efficiently ionized into higher charge states. As there is a reduction in the number of N^+, yet an increase in N II intensity, it is hypothesized that the kinetic energy gained by the dissociation fragments of N_2 molecules provides better access to plasma regions where T_e and n_e produce higher N II emission per N^+ ion. The time-averaged, volume-integrated number of multiply charged nitrogen ions in the plasma increases by up to a factor of five (N^{7+}) if molecular recycling is assumed. The increase in the N III, N IV and N V intensities predicted by ERO2.0 can thus be explained by an increase in the number of ions in those charge states.

VIII. Conclusions

EDGE2D-EIRENE simulations of nitrogen-seeded JET L-mode plasmas are found to be highly sensitive to the upstream electron density: a 5% decrease in $n_{e,\,sep,\,LFS\text{-}mp}$ increases the electron temperature along the divertor leg causing the N II emission peak to move from next to the X-point to approximately half-way between the X-point and the target. The EDGE2D-EIRENE plasma solutions are by and large insensitive to the cross-field particle diffusivity for nitrogen ions, and an increase from 1.0 to 10.0 m^2s^{-1} yields only a factor of two increase in the peak line intensity for N III. The emission profile widths are unaffected by the increase in $D_{\perp,\,N}$. EDGE2D-EIRENE reproduces the peak N I to N V line intensities to within 50% of the experimentally measured values. In ERO2.0, this agreement is reduced when only nitrogen atoms are included, or when assuming that the only source of nitrogen molecules is gas injection. However, when nitrogen ions are assumed to recycle as molecules, and atoms assumed to recombine into molecules upon surface impact, agreement between the experimentally measured and ERO2.0 predicted peak N II to N V line intensities to within

50% is achieved. It is unlikely that nitrogen ions would recycle exclusively as N_2 molecules in a primarily deuterium plasma, and in nitrogen-seeded deuterium discharges at JET it has been shown that e.g. ND radicals are formed [27]. However, the dissociative ionization of NH^+, for example, has been shown to produce N^+ ions with similar translational energies as the dissociative ionization N_2^+ molecules [28].

The results in this paper suggest the possibility that the agreement between EDGE2D-EIRENE and the experiment is coincidental due to the combination of overestimating the temperature gradient forces and not including nitrogen molecules. However, the agreement between ERO2.0 and experiment decreases for N I when molecular recycling is assumed. When estimating N I emission, only electron-impact excitation is accounted for by ERO2.0, and therefore other possible sources of N I emission should be included in the code, such as free-electron recombination (contributing ca. 10% in the EDGE2D-EIRENE simulations) and molecular processes like dissociative excitation [29].

Acknowledgements

This work has been carried out within the framework of the EUROfusion Consortium, funded by the European Union via the Euratom Research and Training Programme (Grant Agreement No 101052200 — EUROfusion). Views and opinions expressed are however those of the author(s) only and do not necessarily reflect those of the European Union or the European Commission. Neither the European Union nor the European Commission can be held responsible for them. This work made use of the Triton cluster, part of the Science-IT project at Aalto University.

[1] M. Bernert et al., "X-point radiation, its control and an ELM suppressed radiating regime at the ASDEX Upgrade tokamak," *Nuclear Fusion,* vol. 61, p. 024001, 2021.

[2] A. Huber et al., "Peculiarity of highly radiating multi-impurity seeded H-mode plasmas on JET with ITER-like wall," *Physica Scripta,* vol. T171, p. 014055, 2020.

[3] D. Neuwirth et al., "Formation of ammonia during nitrogen-seeded discharges at ASDEX Upgrade," *Plasma Physics and Controlled Fusion,* vol. 54, p. 085008, 2012.

[4] M. Oberkofler et al., "First nitrogen-seeding experiments in JET with the ITER-like Wall," *Journal of Nuclear Materials,* vol. 438, pp. S258-261, 2013.

[5] R. Pitts et al., "Physics basis for the first ITER tungsten divertor," *Nuclear Materials and Energy,* vol. 20, p. 100696, 2019.

[6] C. Giroud et al., "High Performance ITER-baseline discharges in deuterium with nitrogen and neon-seeding in the JET-ILW," in *Proc. 28th IAEA Fusion Energy Conf.*, 2021.

[7] R. Simonini et al., "Models and numerics in the multi-fluid 2-d edge plasma code EDGE2D/U," *Contributions to Plasma Physics,* vol. 34, p. 368–373, 1994.

[8] D. Reiter et al., "The EIRENE and B2-EIRENE codes," *Fusion Science and Technology,* vol. 47, p. 172–186, 2005.

[9] B. Lomanowski et al., "Spectroscopic investigation of N and Ne seeded induced detachment in JET ITER-like wall L-modes combining experiment and EDGE2D modeling," *Nuclear Materials and Energy,* vol. 20, p. 100676, 2019.

[10] J. Romazanov et al., "First ERO2.0 modeling of Be erosion and non-local transport in JET ITER-like wall," *Physica Scripta,* vol. T170, p. 014018, 2017.

[11] R. Mäenpää et al., "Nitrogen molecular break-up and transport simulations in the JET divertor," in *European Physical Society Conference on Plasma Physics*, 2021.

[12] M. Reinke et al., "Expanding the role of impurity spectroscopy for investigating the physics of high-Z dissipative divertors," *Nuclear Materials and Energy,* vol. 12, pp. 91-99, 2017.

[13] C. Maggi et al., "A new visible spectroscopy diagnostic for the JET ITER-like wall main chamber," *Review of Scientific Instruments,* vol. 83, p. 10D517, 2012.

[14] A. Meigs et al., "Enhancement of JET's mirror-link near-ultraviolet to near-infrared divertor spectroscopy system," *Review of Scientific Instruments,* vol. 81, p. 10E532, 2010.

[15] K. Lawson et al., "Enhancements to the JET poloidally scanning vacuum ultraviolet/visible spectrometers," *Review of Scientific Instruments,* vol. 83, p. 10D536, 2012.

[16] A. Huber et al., "Development of a mirror-based endoscope for divertor spectroscopy on JET with the new ITER-like wall," *Review of Scientific Instruments,* vol. 83, p. 10D511, 2012.

[17] J. Karhunen et al., "Effect of reflections on 2D tomographic reconstructions of filtered cameras and on interpreting spectroscopic measurements in the JET ITER-like wall divertor," *Review of Scientific Instruments,* vol. 90, p. 103504, 2019.

[18] P. Morgan et al., "Spectroscopic measurements on the Joint European Torus using optical fibers to relay visible radiation," *Review of Scientific Instruments,* vol. 56, p. 862, 1985.

[19] M. Groth et al., "Impact of carbon and tungsten as divertor materials on the scrape-off layer conditions in JET," *Nuclear Fusion,* vol. 53, p. 093016, 2013.

[20] J. Miettunen et al., "Dissociation of methane and nitrogen molecules and global transport of tracer impurities in an ASDEX Upgrade L-mode plasma," *Plasma Physics and Controlled Fusion,* vol. 56, p. 095029, 2014.

[21] P. Cosby, "Electron-impact dissociation of nitrogen," *The Journal of chemical physics,* vol. 98, p. 9544–9553, 1993.

[22] D. Rapp et al., "Cross sections for dissociative ionization of molecules by electron impact," *The Journal of chemical physics,* vol. 42, p. 4081–4085, 1965.

[23] E. Bahati et al., "Electron impact dissociation and ionization of N2+," *Journal of Physics B: Atomic, Molecular and Optical Physics,* vol. 34, p. 2963, 2001.

[24] Y. Homma and A. Hatayama, "Numerical modeling of the thermal force in a plasma for test-ion transport simulation based on a Monte Carlo Binary Collision Model (II) – Thermal forces due to temperature gradients parallel and perpendicular to the magnetic field," *Journal of Computational Physics,* vol. 250, pp. 206-223, 2013.

[25] D. Reiser et al., "Improved kinetic test particle model for impurity transport in tokamaks," *Nuclear Fusion,* vol. 38, p. 165, 1998.

[26] P. Stangeby, The Plasma Boundary of Magnetic Fusion Devices, Bristol and Philadelphia: Institute of Physics Publishing, 2000, pp. 303, 335-336.

[27] E. Pawelec et al., "Molecular ND Band Spectroscopy in the Divertor Region of Nitrogen Seeded JET Discharges," *Journal of Physics: Conference Series,* vol. 959, p. 012009, 2018.

[28] J. Lecointre et al., "Electron-impact dissociation and ionization of NH+: formation of N+ and N2+," *Journal of Physics B: Atomic, Molecular and Optical Physics,* vol. 43, p. 105202, 2010.

[29] R. Filippelli et al., "Production of atomic nitrogen emission by electron-impact dissociative excitation of nitrogen molecules," *Journal of Chemical Physics,* vol. 76, p. 3597, 1982.

Appendix A

$n_{e,sep,LFS\text{-}mp}$ / $D_{\perp,N}$	1.0 m²/s	2.0 m²/s	5.0 m²/s	10.0 m²/s
$2.000 \cdot 10^{19}$ m^{-3}	apr2622/seq#1	apr2622/seq#3	apr2622/seq#4	apr2622/seq#5
$1.950 \cdot 10^{19}$ m^{-3}	mar0622/seq#3	mar1422/seq#2	apr2122/seq#1	apr2122/seq#2
$1.900 \cdot 10^{19}$ m^{-3}	mar0622/seq#2	mar1022/seq#1	mar1022/seq#2	mar1122/seq#2

Table 1: List of EDGE2D-EIRENE catalogue names as stored on the JET Linux cluster Heimdall (as of May 17, 2022). Prepend all names with “rmaenpaa/edge2d/jet/81472/”.

Figure captions

Fig.1 a) Tomographic reconstruction of N II emission at 500.6 nm during JET pulse 90423 (15.5-16.5 s). b) Poloidal distribution of N II emission at 500.6 nm from the EDGE2D-EIRENE post-processor pyproc for $n_{e,\,sep,\,LFS\text{-}mp} = 2.0 \cdot 10^{19}$ m^{-3} and $D_{\perp,\,N} = 1.0$ m^2 s^{-1}. c) Poloidal distribution of N II emission at 500.6 nm from the EDGE2D-EIRENE post-processor pyproc for $n_{e,\,sep,\,LFS\text{-}mp} = 1.9 \cdot 10^{19}$ m^{-3} and $D_{\perp,\,N} = 1.0$ m^2 s^{-1}. Separatrix marked in red in a)-c). Vertically viewing divertor spectrometer (KT3) lines of sight marked in white.

Fig. 2 Radial profile of N II 500.6 nm line intensity measured by the fiber optic outer divertor spectrometer system (KS3O), corresponding synthetic measurement based on the tomographic reconstruction in Fig. 1 a) and the prediction from EDGE2D-EIRENE post-processor pyproc for $n_{e,\,sep,\,LFS\text{-}mp} = 1.9 \cdot 10^{19}$ m^{-3} and $D_{\perp,\,N} = 1.0$ m^2 s^{-1}. Error bars represent standard deviations over time points.

Fig. 3 Radial profile of line intensity of N II (a), N III (b) and N IV (c) measured by the high-resolution, vertically viewing divertor spectrometer (KT3), prediction from the EDGE2D-EIRENE post-processor pyproc and predictions from the three ERO2.0 cases for $n_{e,\,sep,\,LFS\text{-}mp} = 1.9 \cdot 10^{19}$ m^{-3} and $D_{\perp,\,N} = 1.0$ m^2 s^{-1}. Error bars represent standard deviations over time points (measurement) and time steps (simulations).

Fig. 4 Line intensity of N I and N II (triangles and spheres, respectively) spectral lines from the low resolution, vertical divertor LFS target viewing spectrometer (KS8D) measurement, prediction from the EDGE2D-EIRENE post-processor pyproc and predictions from the three ERO2.0 cases for $n_{e,\,sep,\,LFS\text{-}mp} = 1.9 \cdot 10^{19}$ m^{-3} and $D_{\perp,\,N} = 1.0$ m^2 s^{-1}. Note the different vertical axis for N II 500.6 nm line intensity. Error bars represent standard deviations over time points (measurement) and time steps (simulations).

Fig. 5 Radial profile of line intensity of N V measured by the poloidally scanning extreme ultraviolet spectrometer (KT1), prediction from the EDGE2D-EIRENE post-processor pyproc

and predictions from the three ERO2.0 cases for $n_{e,\,sep,\,LFS\text{-}mp} = 1.9{\cdot}10^{19}$ m^{-3} and $D_{\perp,\,N} = 1.0$ m^2 s^{-1}. Error bars represent standard deviations over time points (measurement) and time steps (simulations).

Fig. 6 Time-averaged, volume-integrated number of nitrogen ions by charge state from the three ERO2.0 cases. Note the different vertical axis for N^+. Error bars represent standard deviations over time points (measurement) and time steps (simulations).

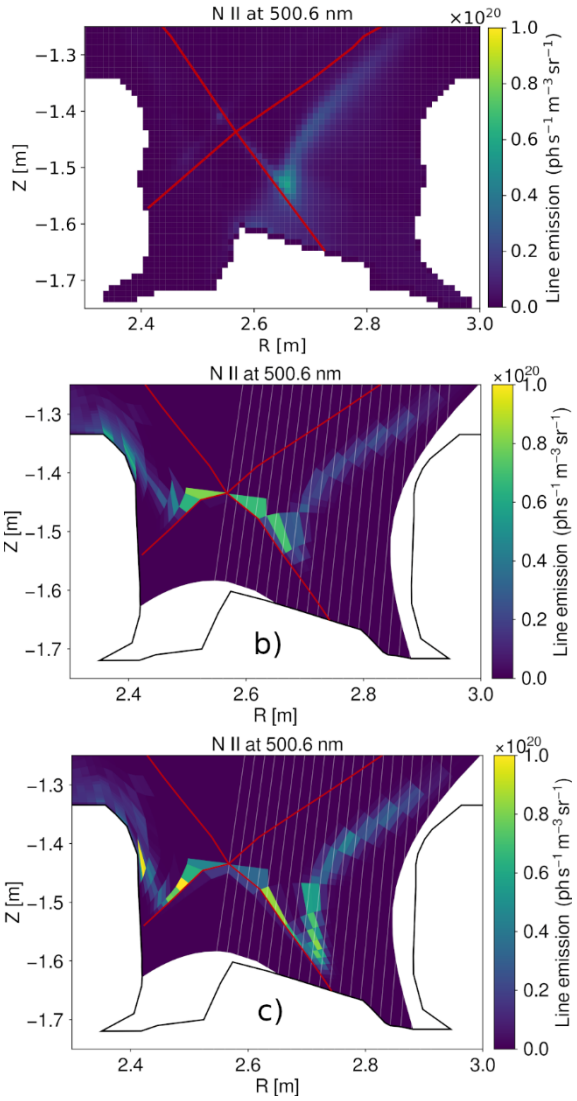

Fig. 1, R. Mäenpää et al. PSI 2022 – one-column 7.5 cm / 14.5 cm = 290 words

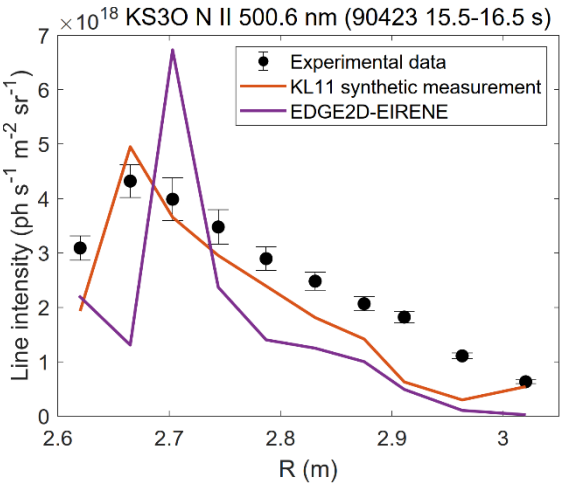

Fig. 2, R. Mäenpää et al. PSI 2022 – one-column 7.5 cm / 6.3 cm = 126 words

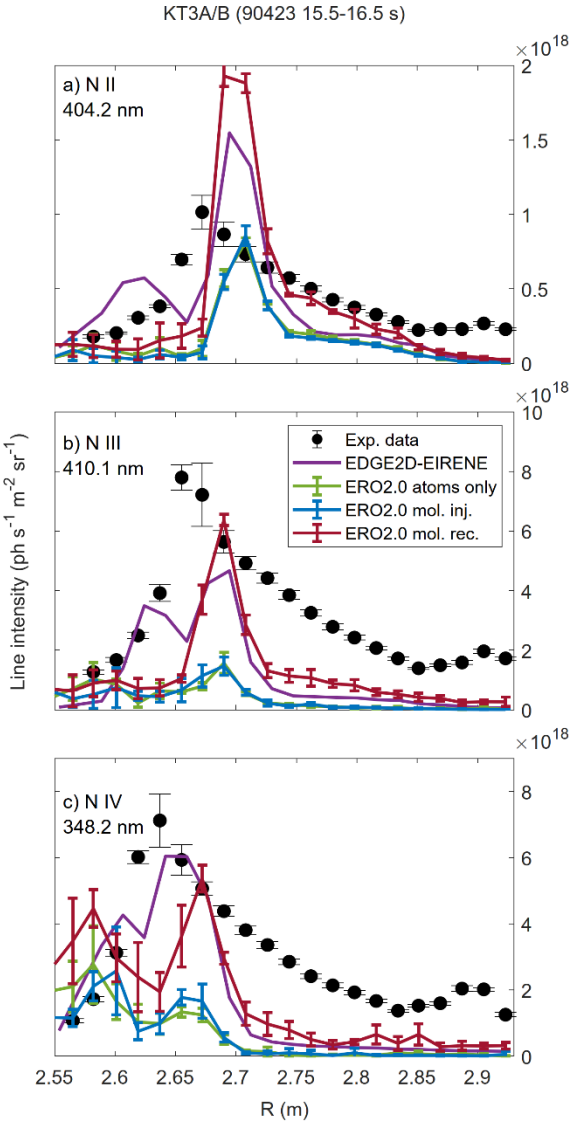

Fig. 3, R. Mäenpää et al. PSI 2022 – one-column 7.5 cm / 14.8 cm = 296 words

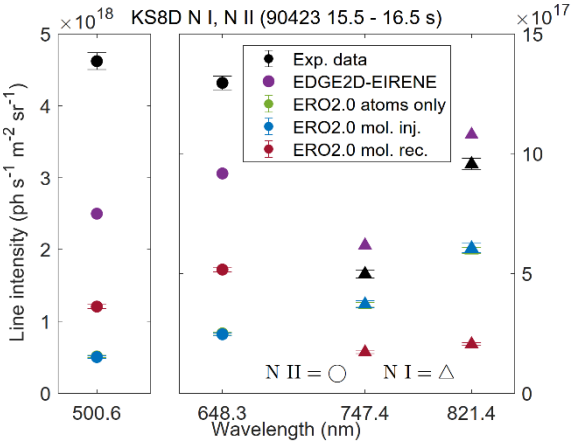

Fig. 4, R. Mäenpää et al. PSI 2022 – one-column 7.5 cm / 5.8 cm = 116 words

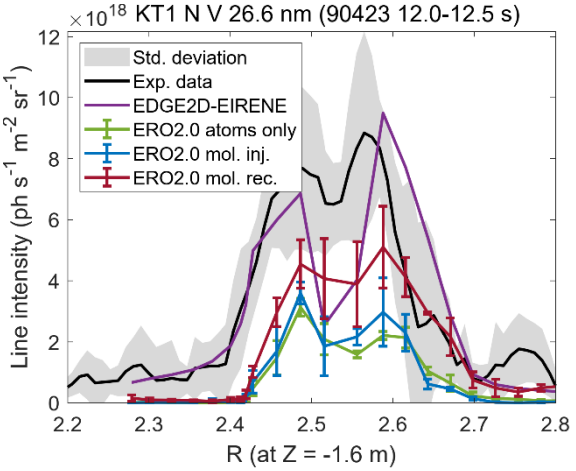

Fig. 5, R. Mäenpää et al. PSI 2022 – one-column 7.5 cm / 6.2 cm = 124 words

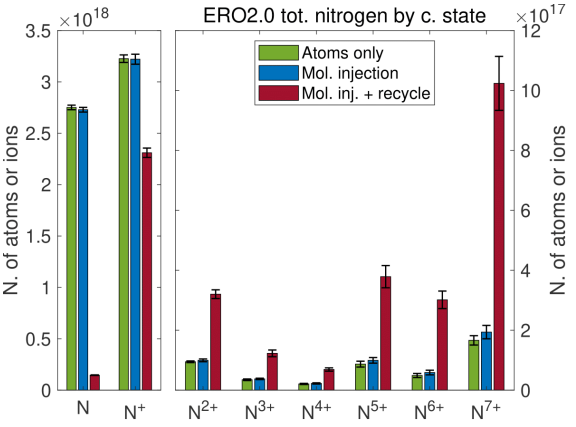

Fig. 6, R. Mäenpää et al. PSI 2022 – one-column 7.5 cm / 5.5 cm = 110 words

The length of the manuscript is computed in terms of the number of single-column journal width lines.

Limits: 5500 words (oral/poster)

Body text, including text, title, abstract = 4533

Table 1 = two columns 16 cm / 4 cm = 160 words

Fig. 1 = 290
Fig. 2 = 126
Fig. 3 = 296
Fig. 4 = 116
Fig. 5 = 124
Fig. 6 = 110

Figure captions = 396

Total words for figure w/o captions = 1062, w/ caption = 1458

NOTE: TOTAL LINES FOR YOUR MS =

Draft 1: 6151 words